Beyond the tubule: Pathologic variants of *LRP2*, encoding the megalin receptor, result in glomerular loss and early progressive chronic kidney disease

Jennifer R Charlton[1*], Weizhen Tan[2*], Ghaleb Daouk[2], Lisa Teot[3], Seymour Rosen[3,4], Kevin M Bennett[5], Aleksandra Cwiek[1**], Sejin Nam[6], Francesco Emma[7], François Jouret[8], João Paulo Oliveira[9], Lisbeth Tranebjærg[10,11], Carina Frykholm[12], Shrikant Mane[13], Friedhelm Hildebrandt[14], Tarak Srivastava[15], Tina Storm[16], Erik Ilsø Christensen[16], Rikke Nielsen[16]

[1]Division of Nephrology, Department of Pediatrics, University of Virginia, Charlottesville, VA, USA
[2]Division of Nephrology, Massachusetts General Hospital for Children, Boston, MA, USA
[3]Department of Pathology, Boston Children's Hospital, Boston, MA, USA
[4]Department of Pathology, Beth Israel Deaconess Medical Center, Boston, MA, USA
[5]Department of Radiology, Washington University in Saint Louis, St. Louis, MO, USA
[6]Department of Physics, University of Hawai'i at Manoa, HI, USA
[7]Division of Nephrology, Department of Pediatric Subspecialties, Bambino Gesù Children's Hospital - IRCCS, Rome, Italy
[8]Groupe Interdisciplinaire de Génoprotéomique Appliquée (GIGA), Unit of Cardiovascular Sciences, University of Liège (ULiège), Liège, Belgium
[9]Service of Medical Genetics, São João University Hospital Centre & Faculty of Medicine, University of Porto and i3S – Institute for Health Research and Innovation (*Instituto de Investigação e Inovação em Saúde*), Porto, Portugal
[10]Department of Clinical Genetics, Rigshospitalet/The Kennedy Centre, Copenhagen, Denmark
[11]Institute of Clinical Medicine, University of Copenhagen, The Panum Institute, Copenhagen, Denmark
[12]Department of Immunology, Genetics and Pathology, Uppsala University, Uppsala, Sweden
[13]Department of Genetics, Yale University School of Medicine, New Haven, CT, USA
[14]Department of Medicine, Boston Children's Hospital, Harvard Medical School, Boston, MA, USA
[15]Children's Mercy Hospital, Kansas City MO, USA
[16]Department of Biomedicine, Aarhus University, Aarhus, Denmark
[*]Shared authorship
[**]On leave from University of Warsaw, Warsaw, Poland

Running title: Megalin and chronic kidney disease

Corresponding author:
Rikke Nielsen
Department of Biomedicine
Aarhus University
8000 Aarhus, Denmark
Mobile: +4527782817
e-mail : rn@biomed.au.dk

SUPPLEMENTAL MATERIAL
https://figshare.com/s/9457ba7cd91ce882bb32
https://doi.org/10.6084/m9.figshare.12993152

Key words: Kidney disease aetiology, megalin, proximal tubule, nephron loss, nephron mass, CFE-MRI, glomerular number

ABSTRACT

Pathogenic variants in the *LRP2* gene, encoding the multiligand receptor megalin, cause a rare autosomal recessive syndrome: Donnai-Barrow/Facio-Oculo-Acoustico-Renal (DB/FOAR). Due to the rarity of the syndrome, the long-term consequences of the tubulopathy on human renal health have been difficult to ascertain and the human clinical condition has hitherto been characterized as a benign tubular condition with asymptomatic low-molecular-weight proteinuria.

We investigated renal function and morphology in a murine model of DB/FOAR syndrome and in DB/FOAR patients. We analyzed glomerular filtration rate (GFR) in mice by FITC-inulin clearance and clinically characterized six families including nine DB/FOAR patients and nine family members. Urine samples from patients were analyzed by western blotting and biopsy material by histology. In the mouse model, we used histologic methods to assess nephrogenesis and post-natal renal structure, and contrast-enhanced magnetic resonance imaging to assess glomerular number.

In megalin deficient mice, we found a lower GFR and an increase in the abundance of injury markers such as kidney injury molecule-1 and NAGase. Renal injury was validated in patients, who presented with increased urinary kidney injury molecule-1, classical markers of chronic kidney disease and glomerular proteinuria early in life. The megalin deficient mice had normal nephrogenesis, but they had 19% fewer nephrons in early adulthood and an increased fraction of nephrons with disconnected glomerulotubular junction.

In conclusion, megalin dysfunction as present in DB/FOAR syndrome confers an increased risk of progression into chronic kidney disease.

The autosomal recessive Donnai-Barrow/Facio-Oculo-Acoustico-Renal (DB/FOAR) syndrome is caused by pathogenic variants in the *LRP2* gene, encoding the receptor megalin (20). Megalin is a 600 kDa endocytic receptor present in low amounts in podocytes and abundant at the apical membrane of the renal proximal tubule. It is also located in many extrarenal epithelia such as the eye, choroid plexus, ear, and embryonic tissues, including the neuroectoderm (11, 13, 14, 22, 31, 33, 39, 40, 42, 48, 49). Consequently, patients with pathogenic variants in *LRP2* exhibit a multifaceted phenotype including hypertelorism, anomalies of corpus callosum and high myopia (20). However, reports of patients with only few of the classical DB/FOAR symptoms and pathogenic variants in *LRP2* have been published (2, 34, 44), suggesting a broader phenotype and potentially a higher prevalence of the disease.

The well described, clinical renal phenotype of DB/FOAR patients is a tubular defect resulting in low-molecular-weight proteinuria (20, 41), consistent with the known role of megalin as a multiligand receptor. Megalin, in concert with the receptor cubilin, reabsorbs virtually all filtered proteins from urinary loss by endocytosis in the proximal tubule (12). Patients with *LRP2* pathogenic variants experience urinary loss of vitamin D binding protein (VDBP), retinol binding protein (RBP) and albumin (1, 27, 41, 46, 47), similar to mouse models with megalin deletion in the kidney (27, 46). Interestingly, urinary loss of low-molecular weight proteins is reported in DB/FOAR patients no matter of the severity of the disease, and a glomerular phenotype has been observed in a few patients (24, 35, 38). Our aim was to establish if the renal phenotype of this classical tubular disease increases the risk of a glomerular dysfunction and renal decline.

In this study, we show kidney injury and a decline in function, in a mouse model with embryonic kidney-specific deletion of megalin mimicking the human phenotype of DB/FOAR syndrome. We provide evidence that DB/FOAR patients develop glomerular proteinuria and chronic kidney disease (CKD) early in life. In the mouse model, we observe that the duration of nephrogenesis is unaffected, but that megalin deficiency results in nephron loss

and abnormalities in the glomerulotubular junction in early adulthood. Our data suggest that megalin is not only an important tubular receptor, but that it is also required for glomerular health.

METHODS

Patients and families

Nine patients (3 months to 35 years of age) from six families were included in the study and family members were included if available (Supplementary material includes a description of each family). Each patient is identified by a two-number label e.g. 1-1, where the first stands for the family and the second for the individual. Family members are also designated “carriers” and presented with the family number and a letter (e.g. 2a). Each individual was coupled to a symbol making it possible to see the location of their pathogenic variant in the protein and their urinary protein excretion in Figure 2.

Urinary protein excretion

Spot urine samples collected from the patients were combined with a protease inhibitor cocktail (Complete; Roche, Denmark) and stored at -80°C. Urinary protein excretion was compared with urinary protein excretion in 5-9 age-matched healthy individuals. A urinary volume corresponding to four µg of creatinine (corresponding to 35 nmol) was analyzed using SDS-PAGE and transferred to an Immobilon™ –FL PVDF transfer membrane (Millipore, Copenhagen, Denmark) using the iBlot™ Dry Blotting System (Invitrogen, Taastrup, Denmark). Membranes were subsequently blocked and incubated with primary and fluorophore-coupled secondary antibodies according to manufacturer (LI-COR Biosciences). Proteins were detected using the Odyssey™ infrared imager (LI-COR Biosciences, Cambridge, United Kingdom). Urinary albumin, creatinine and protein were additionally measured in certified biochemical laboratories in the specific countries.

Immunohistochemistry

Renal tissue samples collected from patients for diagnostic purposes were fixed and embedded in paraffin for routine pathology. For light microscope immunohistochemistry, sections from the patients and controls were prepared as previously described (45). Sections were incubated with a primary antibody in 0.01 M PBS, 0.1% BSA and 0.02 M NaN_3, followed by incubation with HRP-conjugated secondary antibody. Peroxidase labelling was visualized by incubation with

diaminobenzidine and 0.03% H_2O_2 for 10 min. Sections were counterstained with Meier's haematoxylin stain and examined in a Leica DMR microscope equipped with a Leica DFC320 camera. Images were transferred by a Leica TFC Twain 6.1.0 program and processed using Adobe Photoshop 8.0. Fluorescence microscopy was performed by standard methods.

Antibodies

Primary antibodies: rabbit anti vitamin D-binding protein (A0021), rabbit anti transferrin (A0061), rabbit anti albumin (A0001), rabbit anti retinol-binding protein (A0040), rabbit anti β2-microglobulin (A0072), rabbit anti human IgG (A423) were all polyclonal anti-human antibodies (Dako, Glostrup, Denmark). Goat anti KIM-1 (TIM-1, R&D, USA); goat anti mouse cystatin C (R&D, USA); Biotinylated *Lotus tetragonolobus* (*Lotus*) lectin (Vector Labs, B-1325, USA); rabbit anti-horse spleen ferritin antibody (Sigma Aldrich, MO, USA, F6136) and mouse anti-synaptopodin antibody (Santa Cruz Biotechnology SC-21537). Rabbit anti rat cubilin (26); rabbit anti human megalin (31) (kindly provided by Dr. S.K. Moestrup); and sheep anti rat megalin (kindly provided by Dr. P Verroust). Secondary antibodies: IRDye®- (LI-COR), Alexa Fluor®- (Invitrogen), and HRP-conjugated (Dako, Denmark).

Animals

Animal experiments and breeding were approved by the Danish Animal Experiments Inspectorate and performed in the animal facility of Department of Biomedicine, Aarhus University, Denmark. The study adheres to the NIH Guide for the Care and Use of Laboratory animals. Female mice with homozygous conditional inactivation of the *Lrp2* gene in the kidney were generated by breeding Tg(Wnt4-Cre)129SvE-F Tac IK or Tg(Wnt4-Cre)C57BL/6JTac transgenic mice with mice bearing a loxP-flanked Lrp2 allele ($Lrp2^{tm1Tew}$) to create embryonic kidney specific megalin knockout (KO) mice both on a pure C57BL/6JTac – and a pure 129SvE-F Tac IK background. Embryonic Wnt4 expression occurs in tubular cells and podocytes (36, 46). An outline of the number of animals and strain used in each experiment is given in Supplementary Table 1. *Cre*-negative littermates served as controls in all experiments. The KO degree was determined by RT-q-PCR, but when both kidneys were used for other analyses,

159 the KO degree was determined by immunohistochemical analyses. In general, we observed
160 80-95% deletion of megalin, but five animals included in the structural analyses had KO
161 degrees in the range 40-80%.

162 **Mouse kidney function analyses**

163 GFR were investigated by the method of Rieg et al. (32), using intravenous injections of FITC-
164 inulin per gram bodyweight and measurement of plasma clearance of 60-98 days old mice. The
165 weight of the mice did not differ significantly. Plasma and urine creatinine were determined
166 according to standard procedures (Siemens Diagnostics® Clinical Methods for ADVIA 1800)
167 (Jaffe, 74016). Analyses were performed using an autoanalyzer, ADVIA 1800 Chemistry
168 System (Siemens Medical Solutions, Tarrytown, NY 10591, USA). Relative abundance of KIM-
169 1 in urine was measured by Western blotting according to creatinine. N-acetyl-b-D-
170 glucosaminidase (NAGase) activity in urine was detected by an end point fluorometric method,
171 according to Larsen et al. (25).

172 **Cationic ferritin-enhanced magnetic resonance imaging (CFE-MRI)**

173 To label the glomeruli for MRI detection, the mice received 5.75 mg/100 g body weight of horse
174 spleen cationic ferritin (CF) (Sigma Aldrich F7879, MO) at the age of 50-70 days (4, 8). The CF
175 was administered in 2 equal retro-orbital injections separated by 90 minutes under isoflurane
176 anesthesia (4). All animals were euthanized 90 minutes after the last injection of CF followed
177 by retro-aortic perfusion of Hanks buffered salt solution, followed by perfusion with 2% PFA in
178 0.1 M cacodylate buffer, pH 7.4. One kidney was stored whole in 2% glutaraldehyde/0.1 mol/L
179 cacodylate solution for CFE-MRI, the other was post-fixed with formalin for paraffin embedment.
180 The intact kidney was placed in a customized holder with the capacity to image 8 kidneys using
181 a Bruker quadrature RF probe (inner diameter=30 mm). Imaging was performed on a Bruker
182 7T/30 MRI (Bruker, Co., Billerica, MA, USA) with Siemens software for acquisition and
183 reconstruction (Siemens, Munich, Germany) at the University of Virginia (sequence
184 parameters: 3D T2*-weighted scan: TE/TR: 20/80 ms, slice thickness: 60 µm, 640x640). The
185 CF-labeled glomeruli appear as dark spots in the cortex of gradient-echo MR images. This

appearance is consistent with previous publications in mouse (4), rat (7), rabbit (9) and *ex vivo* human (6) MRI, where CF accumulates in the glomerular basement membrane (Supplementary material Figure S1).

Image processing for number and volume of glomeruli N_{glom} and V_{glom}

As in previous publications (4), the images were manually segmented to separate each kidney from the remaining eight and to remove the medullary region. This allows for the measurement of cortical and medullary volumes. The resolution was increased by linear interpolation to 19.53 x 19.53 x 20 mm using Amira (FEI, Bordeaux, France) software. 3D raw data of the segmented kidney were processed in Matlab (The Mathworks, Inc. Nantick, MA, USA) to create two sets of 2D images along the x and y axes. MIPAR was used to manually adjust contrast (low level, high level, and γ values of 2, 128, and 1.5 respectively). Kidney images were processed using an adaptive thresholding in MIPAR with a threshold of 50 percent and a window size of 15 pixels. Segmented glomeruli smaller than four voxels were rejected. The glomerular images and segmented medulla regions were analyzed with custom MATLAB scripts to obtain number of glomeruli (N_{glom}) and apparent volume of glomeruli (aV_{glom}) as previously described (4).

Validation of CF labeling

Immunofluorescence was performed on formalin fixed kidney tissue from the contralateral kidney that underwent MRI to confirm targeted CF labeling in the glomeruli (Supplementary material Figure S1). Kidney samples were embedded in paraffin, sectioned at four microns thick, rehydrated using Histoclear (National diagnostics, GA) and graded ethanol dilutions. Antigen retrieval was accomplished by boiling the slides in a 10 mM citrate buffer. The tissue was blocked using normal donkey serum 1:10 in 5% of BSA in PBS for 1 hour in a humidity chamber. The sections were incubated with the following primary antibodies overnight (1) rabbit anti-horse spleen ferritin antibody (*concentration -1:100*, Sigma Aldrich, St. Louis, MO, USA, F6136) and (2) mouse anti-synaptopodin antibody to highlight the podocytes (*concentration - 1:*200). Secondary antibodies were applied for 2 hours at room temperature: donkey anti-rabbit Alexa 594 (1:200, Life Technologies) and donkey anti-mouse Alexa 488 (1:250, Life

Technologies). To stain the nuclei, 4',6-diamidino-2-phenylindole (DAPI) was applied and each slide was rehydrated. Images were obtained using Microscope Leica Microsystems CMS GmbH.

Histologic assessment

Kidney samples from the 50-70 day group were prepared by standard techniques, embedded in paraffin and sectioned. The presence of *Lotus* lectin (Vector Laboratories) was identified in by treating sections with proteinase K enzymatic digestion followed by biotinylated *Lotus* lectin (1:50 dilution) and the ABC-DAB reaction was induced). Quantitation of the proximal tubules was accomplished by analyzing the DAB reaction within each image (ImagePro Plus 5.1, Media Cybernetics, Silver Springs, MD). Renal cortical volume fraction of proximal tubules was measured using a stereologic approach as described in previous publications (18). Ten fields were photographed at 20x magnification in the subcapsular region and the DAB reaction product was expressed as a percent area value (volume fraction [V_v]). As *Lotus* lectin staining is specific to the mature proximal tubular cells and papillary collecting duct, the identification of the *Lotus* positive area is useful for quantifying the preservation of the renal cortex and the lack of staining present in Bowman's capsule represents disruption of the glomerulotubular connection ("atubular glomeruli"). In essence, the latter fraction includes both real atubular glomeruli and glomeruli assessed at a plane where the junction is not visible. Comparison of the *Lotus* lectin negative glomeruli in the two groups indicates whether there is an increase in real atubular glomeruli in either group. This method has been extensively validated in serial sections (18).

Neonatal cohort

It is not feasible to do CFE-MRI on neonatal mouse kidneys, therefore the kidneys were prepared and stained with Periodic Acid Schiffs (PAS) to identify glomeruli. Mature glomeruli were counted in a mid-sagittal section at the completion of nephrogenesis, postnatal day four. Using Amira Software (FEI, Bordeaux, France), a 3D visualization program, the cortical area was determined from each sample. Glomerular density was defined as mature

glomeruli/cortical area. To determine duration of the nephrogenic zone, kidney sections were stained with *Lotus* lectin to identify the presence of a nephrogenic zone. Cessation of the nephrogenic zone was defined by a lack of cap mesenchyme and the presence of *Lotus* lectin stained cells just under the capsule.

Study approval

The study was performed according to the Declaration of Helsinki and approved by the National Ethical Review Boards. Informed consent was obtained from all participants.

Statistics

For analyses of urine content in patients, a one-way ANOVA was used if the populations were normally distributed evaluated by a D'Agostino & Pearson normally test and had variance homogeneity. The number of patients in the DB/FOAR group was too small to analyze for normal distribution. If the groups were not normally distributed or did not have a positive test for variance homogeneity, a non-parametric Kruskal-Wallis test with a Dunn's test for multiple comparisons was performed. When two groups were compared, a Students t-test was performed in case of normal distribution and a Mann-Whitney test was performed otherwise.

RESULTS

Renal injury and decline of renal function in murine megalin deficiency.

We investigated the role of megalin on renal function in a mouse model of DB/FOAR syndrome. The model is obtained by embryonic kidney-specific knockout of megalin (megalin KO) (36, 46). In the adult mice, we found a reduced kidney function evidenced by decreased GFR (mean ± SEM KO: 287 ± 25 μl/min vs. wildtypes (WT): 368 ± 26 μl/min, p=0.04) and slightly increased plasma creatinine (mean ± SEM KO: 14.4 ± 1.2 μmol/l vs. WT: 11.2 ± 0.8 μmol/l, p=0.04) (Figure 1, A and B). At this young age, the renal parenchyma from some megalin KO mice revealed areas lacking proximal tubules (Figure 1C). In megalin KO mice, we have previously reported urinary excretion of kidney injury markers such as cystatin C (30). As these are megalin ligands we also investigated injury markers in the urine that are not megalin ligands, which were also elevated in the megalin KO mice as compared to WT including N-acetyl-beta-D-glucosaminidase (NAGase: mean ± SEM KO: 0.08 ± 0.013 U/μmol creatinine vs. WT: 0.005 ± 0.0002 U/μmol creatinine, p<0.001) and kidney injury molecule-1 (KIM-1: mean ± SEM KO: 10.8 x 10^6 ± 1.2 x 10^6 AU/ creatinine vs. WT: 1.5 x 10^6 ± 0.3 x 10^6 AU/creatinine, p<0.016) (Figure 1, D and E). These data suggest that megalin deficiency results in renal injury.

DB/FOAR patients demonstrate renal decline

To investigate renal status in the human counterpart of our mouse model, we examined six families with pathogenic variants in the megalin encoding gene, *LRP2*. Four of the six families were newly identified (Table 1, Families 1, 2, 5 and 6). All patients are homozygous for the pathogenic variant indicated in Table 1 and depicted in Figure 2A, whereas carriers are heterozygous for the variant. Clinical data from the patients showed urine protein-creatinine (UP/C) levels in the range 166-704 mg/mmol (normal <15 mg/mmol), albumin-creatinine (UA/C) levels ranging from 7–33 mg/mmol (normal <3 mg/mmol) indicating a glomerular leak and four patients had low GFR (Table 1). Analyses of patient urines showed elevated excretion of classical megalin and cubilin ligands such as RBP (megalin ligand), transferrin (cubilin ligand),

albumin (shared ligand), cystatin C (megalin ligand) and β2-microglobulin (megalin ligand), as compared to controls and carriers (Figure 2B and Supplementary material Figure S2). In addition to low-molecular-weight ligands, we also detected a significantly increased excretion of intact (150 kDa) IgG in all patient urines, indicating an effect on the glomerular filtration barrier (Figure 2B). Thus, in addition to low-molecular-weight proteinuria the patients also demonstrated proteinuria of glomerular origin. Furthermore, elevated presence of kidney injury marker-1 (KIM-1) in all DB/FOAR patients and in three of the carriers from Family 2 (Figure 2B), suggesting renal injury and glomerular dysfunction.

All patients showed a characteristic urinary protein profile, which was different from carriers and controls (Supplementary material Figure S3). As expected, DB/FOAR patients from Families 2, 3, 4 and 6 had almost no full-length megalin excretion in the urine, consistent with the absence of megalin protein products. Surprisingly, urinary full-length megalin was also virtually absent in urines from the carriers (Figure 2B).

Analyses of biopsy material (available from Families 1, 4 and 6), showed no brush border immunoreactivity for megalin in Families 4 (41) or 6 (Figure 3A), which has also previously been shown in family 3 (15). Surprisingly, the two index patients from Family 1 had reduced, normally localized megalin (Figure 3A). Consistent with the remnant presence of the receptor in patients from Family 1, we detected uptake of ligands like RBP and albumin (Figure 3A), which was not present in Families 4 (41) or 6 (Figure 3A). Despite the presence of immunodetectable ligands in patients from Family 1, they also presented with proteinuria (Table 1; unfortunately, urine was inaccessible for further analyses). The presence of proteinuria could be caused by a combination of suboptimal reabsorption (compatible with reduced megalin) and increased glomerular protein leakage. PAS staining of kidney biopsy material from Patient 1-1 revealed chronic changes including focal glomerulosclerosis, interstitial fibrosis, inflammation and tubular atrophy (Figure 3B). In contrast, Patient 1-2 had fairly well-preserved renal parenchyma (Figure 3B), but the glomeruli from both Patients of Family 1 showed signs of advanced renal disease. Some glomeruli were sclerotic, whereas others appeared normal

(Figure 3B). Immunofluorescence revealed immunoglobulin A deposits in all glomeruli investigated in Patient 1-2 and a more focal pattern in Patient 1-1 (Figure 3B). In summary, megalin dysfunction in DB/FOAR patients is associated with proteinuric CKD with glomerular and tubulointerstitial histological lesions.

Nephrogenesis is normal in the megalin deficient kidney.

Megalin is present early in nephrogenesis, which makes it possible that the fully functioning receptor is needed for proper regulation of kidney development through binding and clearing of regulating proteins such as sonic hedgehog (28, 29). To investigate the mechanism underlying renal decline, we investigated central parameters in nephrogenesis. We examined a cohort of neonatal mice (n=3/group from postnatal (PN) days 0-4) and found that cessation of the nephrogenic zone occurred on postnatal day four in both the megalin KO and WT groups as evidenced by a lack of cap mesenchyme and the presence of *Lotus* lectin stained cells just under the capsule (Figure 4A). Furthermore, we found that there was no difference in glomerular density at postnatal day four between the KO and WT mice (mean ± SEM KO: 1.3 ± 0.1/μm^2 x10^3 vs. WT: 1.2 ± 0.27/μm^2 x10^3, p=0.40) (Figure 4B) indicating apparent normal nephrogenesis in megalin KO mice.

Nephron loss and disruption of the glomerulotubular junction in megalin deficiency.

To assess if renal injury resulted in nephron loss in adulthood, we applied CFE-MRI (4, 6-8) to determine number (N_{glom}) and size (aV_{glom}) of the glomeruli in the adult kidney. We found the megalin KO group had significantly fewer glomeruli than the WT (mean ± SEM KO: 9702 ± 219; WT: 12056 ± 427, p<0.001, Figure 5A) at 50-70 days. At one year of age, the deposition of cationic ferritin in glomeruli of KO mice was virtually absent, whereas in WT the deposition appeared normal (Supplementary Figure S1) indicating a change of charge or size selectivity of the filtration barrier of megalin deficient mice. No difference in glomerular volume was observed by MRI (apparent glomerular volume (aV_{glom})) between the megalin KO and WT groups (mean ± SEM KO: 3.3 ± 0.1 mm^3 x10^{-4}; WT: 3.1 ± 0.2 mm^3 x10^{-4}, p=0.62, Figure 5B), and the intrarenal distribution of V_{glom} was unchanged (Figure 5C), indicating there was not a

348 population of small and large glomeruli in either group. The proximal tubule fraction was lower
349 in the megalin KO group compared to WT measured as the area *Lotus*-positive cells in the
350 subcapsular region (mean ± SEM KO: 42 ± 1.2% vs. WT: 46 ± 1.4%, p=0.03, Figure 5D). This
351 is supported by MRI analyses showing smaller kidney volume in megalin KO (mean ± SEM KO:
352 $1.1 \times 10^{11} \pm 5.5 \times 10^{9}$ μm^3 vs. WT: $1.3 \times 10^{11} \pm 4.7 \times 10^{9}$ μm^3, p=0.006, Figure 5E), smaller
353 cortical volume in the megalin KO group (mean ± SEM KO: $6.2 \times 10^{10} \pm 3.1 \times 10^{9}$ μm^3 vs. WT:
354 $7.7 \times 10^{10} \pm 2.7 \times 10^{9}$ μm^3, p=0.002, Figure 5F), but no change in medullary volume between
355 the groups (mean ± SEM KO: $4.8 \times 10^{10} \pm 3.1 \times 10^{9}$ μm^3 vs. WT: $4.9 \times 10^{10} \pm 2.9 \times 10^{9}$ μm^3,
356 p=0.8, Figure 5G). In the 50-70 days group, the health of the glomerulotubular junction was
357 compromised; the fraction of *Lotus* negative glomeruli (true atubular glomeruli + glomeruli cut
358 at a plane not assessing the junction) was greater in the KO than in WT (mean ± SEM KO: 32
359 ± 2.6%; WT: 25 ± 1.5%, p=0.048, Figure 5H). Our findings demonstrate that in a WT mouse
360 *Lotus* lectin is not detectable in Bowman's capsule in approximately 25% of the glomeruli,
361 secondary to the direction of the sectioned tissue. However, in the megalin KO mice, the
362 percentage of *Lotus* negative glomeruli is 7% higher than the WT, reflecting a population of
363 atubular glomeruli. Thus, at 8-10 weeks of age the megalin KO mice have lost approximately
364 19% of their glomeruli and another 7% have an abnormal glomerulotubular junction which will
365 likely result in their loss with time. Taken together these analyses suggest that glomerulotubular
366 disconnection and nephron loss are a result of megalin dysfunction.
367
368
369
370
371
372
373
374

DISCUSSION

In this study, we aimed to establish if megalin deficiency or dysfunction plays a role in progressive kidney disease. We found that renal function was affected by megalin dysfunction both in our mouse model and human subjects (figure 6). The absence of megalin in mice resulted in renal decline, disruption of the glomerulotubular junction and nephron loss early in adulthood without an overt effect on nephrogenesis. To validate the renal decline observed in our mouse model in humans, we included six families with pathogenic variants in *LRP2,* to investigate the impact of these variants on renal health. All patients presented with tubular dysfunction, which was apparent by the urinary loss of megalin-cubilin ligands, consistent with megalin dysfunction. In addition, the patients experienced urinary loss of high-molecular-weight proteins like immunoglobulins and transferrin indicative of an affected glomerular filtration barrier. Supportive of a glomerular component of the proteinuria, the patients had urinary protein and albumin excretion which was higher than that of low-molecular-weight proteinuria. Furthermore, several patients had a low GFR (23) and a clinical diagnosis of CKD. In addition, all patients had elevated levels of urinary KIM-1. Urinary KIM-1 has been correlated with inflammation and proximal tubule injury, and has been shown to be a biomarker of renal injury and risk of CKD (37). All together our data strongly suggest that megalin dysfunction poses an increased risk of renal decline involving both the tubules and glomeruli. Our study is in line with a genome-wide association study showing that single nucleotide polymorphisms in *LRP2* are associated with low GFR (10) and we speculate that milder forms of the disease might contribute to the population of patients with CKD without known aetiology. As megalin is present both in podocytes and tubules, future work will focus on the role of megalin in the glomeruli along with ligand loss as potential contributors to kidney health and their role in CKD progression.

Currently, the role of megalin in podocytes is not entirely clarified. Megalin appears to have endocytic function. It was originally described as the Heyman nephritis antigen in rats (21, 22, 31), but it has not been demonstrated to be involved in human nephritis. In Family 1

immunofluorescence revealed immunoglobulin A deposits; in Patient 1-1 all investigated glomeruli were affected, whereas in Patient 1-2 a more of a focal pattern was present. We speculate that the remnant immunoreactive megalin product may be antigenic in this family. Besides this glomerular change in this family, our patient data demonstrated that the filtration barrier was affected indicating a role of megalin in podocyte health. Significant glomerular changes were also present in our mouse model, where at one year of age the deposition of cationic ferritin in KO was almost absent as compared to controls. As CFE deposition requires a negatively charged filtration barrier and a barrier which retains it, this indicates that the filtration barrier is changed either with regards to charge or size selectivity, which points at a role of megalin in the maintenance of podocyte function. Thus, the lack of megalin in podocytes could potentially contribute to renal decline and the loss of the glomerulotubular junction.

To clarify the underlying mechanism of kidney disease, as we know that megalin is present throughout nephrogenesis (3, 33), we used a mouse model with embryonic kidney-specific megalin KO to investigate if the absence of the receptor influences nephron formation (46). We did not find any significant changes in nephrogenesis or early postnatal glomerular density, but a significant impact on renal structure, renal function and nephron abundance in early adulthood. Thus, our data suggest that nephron survival postnatally is affected in the megalin deficient state, which is in line with an earlier report of increased apoptotic cell numbers in megalin-negative cells observed by Theilig et al. in a mosaic megalin KO model (43). Further work is needed to differentiate the direct effect of the loss of megalin ligands in the urine *versus* the lack of the megalin receptor *per se*. Deficiency of megalin ligands, including the lack of uptake of antiapoptotic proteins such as survivin (19), may play a role in maintenance of the glomerulotubular connection and nephron survival. Recently, it has been shown that albumin loss as the consequence of cubilin variants does not cause kidney disease (5), indicating that the loss of albumin and potentially other cubilin ligands (which are much fewer that megalin ligands) does not affect renal health in humans (30). Thus, further work is necessary to determine if replacement of some specific megalin ligands could improve overall renal health

or if also other yet unknown functions of megalin in both podocytes and the tubules could play a role.

The presence, although in low levels, of immunoreactive megalin and ligands in the proximal tubule of patients 1-1 and 1-2 was rather unexpected. The existence of DB/FOAR patients with megalin expression has also been reported by Kantarci et al. (20), supporting that DB/FOAR syndrome can develop despite the presence of an immunoreactive protein product. The pathogenic variant in Family 1 interferes with the YWTD repeat in an LDL class B domain changing Y into H. In the LDL receptor these repeats are involved in pH-dependent release of ligands in the endosomal compartment (16). It is therefore possible that the variant results in a protein product, but restricts ligand dissociation leading to (i) recycling of the whole ligand – receptor complex and (ii) a disturbed endocytic process. Recently, Flemming et al. (17) demonstrated that the pathogenic variant present in Family 6 interferes with receptor-ligand dissociation and causes aberrant trafficking of megalin for lysosomal degradation. A similar mechanism could play a role in the reduced megalin abundance we observed in Family 1. We cannot exclude that the remnant receptor expression in Family 1 mediates endocytosis, but that this is insufficient to avoid protein leakage into the urine combined with the presence of an affected filtration barrier leading to increased filtration.

In conclusion, our study shows pathogenic variants in *LRP2* as an aetiology for early onset of CKD, which could also include patients without the advanced DB/FOAR phenotype pointing to awareness of this as a cause of CKD without a clear aetiology. We document that megalin dysfunction is associated with proximal tubular and glomerular dysfunction, disruption of the glomerulotubular junction with subsequent nephron loss, which most likely contributes to the development or progression of CKD.

AUTHOR CONTRIBUTIONS

JC, WT, SR, EIC, AC, RN: designed, and conducted experiments; collected, analyzed and interpreted data; generated the figures and co-wrote the manuscript. GD, LT, FE, FJ, JPO, LT, CF, TS: provided human material. TSt, EIC AC, SN, KB, FH, SM: analyzed, collected and interpreted data, and edited the manuscript. All authors approved the manuscript.

ACKNOWLEDGEMENTS

We are grateful for the excellent technical assistance of Hanne Sidelmann, Pia K. Nielsen, Helle Gittens, Inger Kristoffersen and Kimberly deRonde. We also thank the Yale Center for Mendelian Genomics for whole exome sequencing analysis (U54HG006504).

Sources of support included grants from the Danish Medical Research Council, Augustinus Foundation, Edith Waagens og Frode Waagens Foundation, the Novo Nordisk Foundation, Jens Ove Jakobsen Foundation, the Bruker ClinScan 7T MRI in the Molecular Imaging Core, which was purchased with support from NIH grant 1S10RR019911-01 and is supported by the University of Virginia School of Medicine. JRC and KMB receive funding from the NIH/NIDDK: R01DK110622 and R01DK111861. FH receive funding from NIH: DK0668306. FJ is Fellow of the Fonds National de la Recherche Scientifique (FNRS) in Belgium.

CONFLICT OF INTERESTS

The authors have declared that no conflict of interest exists.

REFERENCES

1. **Amsellem S, Gburek J, Hamard G, Nielsen R, Willnow TE, Devuyst O, Nexo E, Verroust PJ, Christensen EI, and Kozyraki R**. Cubilin Is Essential for Albumin Reabsorption in the Renal Proximal Tubule. *J Am Soc Nephrol* 21: 1859-1867, 2010.
2. **Anglani F, Terrin L, Brugnara M, Battista M, Cantaluppi V, Ceol M, Bertoldi L, Valle G, Joy MP, Pober BR, and Longoni M**. Hypercalciuria and nephrolithiasis: Expanding the renal phenotype of Donnai-Barrow syndrome. *Clinical genetics* 94: 187-188, 2018.
3. **Assemat E, Chatelet F, Chandellier J, Commo F, Cases O, Verroust P, and Kozyraki R**. Overlapping expression patterns of the multiligand endocytic receptors cubilin and megalin in the CNS, sensory organs and developing epithelia of the rodent embryo. *Gene Expr Patterns* 6: 69-78, 2005.
4. **Baldelomar EJ, Charlton JR, Beeman SC, Hann BD, Cullen-McEwen L, Pearl VM, Bertram JF, Wu T, Zhang M, and Bennett KM**. Phenotyping by magnetic resonance imaging nondestructively measures glomerular number and volume distribution in mice with and without nephron reduction. *Kidney Int* 89: 498-505, 2016.
5. **Bedin M, Boyer O, Servais A, Li Y, Villoing-Gaude L, Tete MJ, Cambier A, Hogan J, Baudouin V, Krid S, Bensman A, Lammens F, Louillet F, Ranchin B, Vigneau C, Bouteau I, Isnard-Bagnis C, Mache CJ, Schafer T, Pape L, Godel M, Huber TB, Benz M, Klaus G, Hansen M, Latta K, Gribouval O, Moriniere V, Tournant C, Grohmann M, Kuhn E, Wagner T, Bole-Feysot C, Jabot-Hanin F, Nitschke P, Ahluwalia TS, Kottgen A, Andersen CBF, Bergmann C, Antignac C, and Simons M**. Human C-terminal CUBN variants associate with chronic proteinuria and normal renal function. *J Clin Invest* 2019.
6. **Beeman SC, Cullen-McEwen LA, Puelles VG, Zhang M, Wu T, Baldelomar EJ, Dowling J, Charlton JR, Forbes MS, Ng A, Wu QZ, Armitage JA, Egan GF, Bertram JF, and Bennett KM**. MRI-based glomerular morphology and pathology in whole human kidneys. *American journal of physiology Renal physiology* 306: F1381-1390, 2014.
7. **Beeman SC, Zhang M, Gubhaju L, Wu T, Bertram JF, Frakes DH, Cherry BR, and Bennett KM**. Measuring glomerular number and size in perfused kidneys using MRI. *American journal of physiology Renal physiology* 300: F1454-1457, 2011.
8. **Bennett KM, Zhou H, Sumner JP, Dodd SJ, Bouraoud N, Doi K, Star RA, and Koretsky AP**. MRI of the basement membrane using charged nanoparticles as contrast agents. *Magnetic resonance in medicine* 60: 564-574, 2008.
9. **Charlton JR, Baldelomar EJ, deRonde KA, Cathro HP, Charlton NP, Criswell SJ, Hyatt DM, Nam S, Pearl V, and Bennett KM**. Nephron loss detected by MRI following neonatal acute kidney injury in rabbits. *Pediatr Res* 2019.
10. **Chasman DI, Fuchsberger C, Pattaro C, Teumer A, Boger CA, Endlich K, Olden M, Chen MH, Tin A, Taliun D, Li M, Gao X, Gorski M, Yang Q, Hundertmark C, Foster MC, O'Seaghdha CM, Glazer N, Isaacs A, Liu CT, Smith AV, O'Connell JR, Struchalin M, Tanaka T, Li G, Johnson AD, Gierman HJ, Feitosa MF, Hwang SJ, Atkinson EJ, Lohman K, Cornelis MC, Johansson A, Tonjes A, Dehghan A, Lambert JC, Holliday EG, Sorice R, Kutalik Z, Lehtimaki T, Esko T, Deshmukh H, Ulivi S, Chu AY, Murgia F, Trompet S, Imboden M, Coassin S, Pistis G, Harris TB, Launer LJ, Aspelund T, Eiriksdottir G, Mitchell BD, Boerwinkle E, Schmidt H, Cavalieri M, Rao M, Hu F, Demirkan A, Oostra BA, de AM, Turner ST, Ding J, Andrews JS, Freedman BI, Giulianini F, Koenig W, Illig T, Meisinger C, Gieger C, Zgaga L, Zemunik T, Boban M, Minelli C, Wheeler HE, Igl W, Zaboli G, Wild SH, Wright AF, Campbell H, Ellinghaus D, Nothlings U, Jacobs G, Biffar R, Ernst F, Homuth G, Kroemer HK, Nauck M, Stracke S, Volker U, Volzke H, Kovacs P, Stumvoll M, Magi R, Hofman A, Uitterlinden AG, Rivadeneira F, Aulchenko YS, Polasek O, Hastie N, Vitart V, Helmer C, Wang JJ, Stengel B, Ruggiero D, Bergmann S, Kahonen M, Viikari J, Nikopensius T, Province M, Ketkar S, Colhoun H, Doney A, Robino A, Kramer BK, Portas L, Ford I, Buckley BM, Adam M, Thun GA, Paulweber B, Haun M, Sala C, Mitchell P, Ciullo M, Kim SK, Vollenweider P, Raitakari O,**

Metspalu A, Palmer C, Gasparini P, Pirastu M, Jukema JW, Probst-Hensch NM, Kronenberg F, Toniolo D, Gudnason V, Shuldiner AR, Coresh J, Schmidt R, Ferrucci L, Siscovick DS, van Duijn CM, Borecki IB, Kardia SL, Liu Y, Curhan GC, Rudan I, Gyllensten U, Wilson JF, Franke A, Pramstaller PP, Rettig R, Prokopenko I, Witteman J, Hayward C, Ridker PM, Parsa A, Bochud M, Heid IM, Kao WH, Fox CS, and Kottgen A. Integration of genome-wide association studies with biological knowledge identifies six novel genes related to kidney function. *HumMolGenet* 21: 5329-5343, 2012.

11. **Chatelet F, Brianti E, Ronco P, Roland J, and Verroust P**. Ultrastructural localization by monoclonal antibodies of brush border antigens expressed by glomeruli. I. Renal distribution. *Am J Pathol* 122: 500-511, 1986.

12. **Christensen EI, Birn H, Storm T, Weyer K, and Nielsen R**. Endocytic receptors in the renal proximal tubule. *Physiology(Bethesda)* 27: 223-236, 2012.

13. **Christensen EI, Gliemann J, and Moestrup SK**. Renal tubule gp330 is a calcium binding receptor for endocytic uptake of protein. *J Histochem Cytochem* 40: 1481-1490, 1992.

14. **Christensen EI, Nielsen S, Moestrup SK, Borre C, Maunsbach AB, de Heer E, Ronco P, Hammond TG, and Verroust P**. Segmental distribution of the endocytosis receptor gp330 in renal proximal tubules. *Eur J Cell Biol* 66: 349-364, 1995.

15. **Dachy A, Paquot F, Debray G, Bovy C, Christensen EI, Collard L, and Jouret F**. In-depth phenotyping of a Donnai-Barrow patient helps clarify proximal tubule dysfunction. *Pediatric nephrology (Berlin, Germany)* 30: 1027-1031, 2015.

16. **Davis CG, Goldstein JL, Sudhof TC, Anderson RG, Russell DW, and Brown MS**. Acid-dependent ligand dissociation and recycling of LDL receptor mediated by growth factor homology region. *Nature* 326: 760-765, 1987.

17. **Flemming JM, M; Rudolph, IM; Nielsen, R; Storm, T; Christensen, EI; Diecke, S; Emma, F; Willnow, T.** Induced pluripotent stem cell-based disease modeling identifies ligand-induced decay of megalin as a cause of Donnai-Barrow syndrome. *Kidney Int* Accepted: 2020.

18. **Galarreta CI, Grantham JJ, Forbes MS, Maser RL, Wallace DP, and Chevalier RL**. Tubular obstruction leads to progressive proximal tubular injury and atubular glomeruli in polycystic kidney disease. *The American journal of pathology* 184: 1957-1966, 2014.

19. **Jobst-Schwan T, Knaup KX, Nielsen R, Hackenbeck T, Buettner-Herold M, Lechler P, Kroening S, Goppelt-Struebe M, Schloetzer-Schrehardt U, Furnrohr BG, Voll RE, Amann K, Eckardt KU, Christensen EI, and Wiesener MS**. Renal uptake of the antiapoptotic protein survivin is mediated by megalin at the apical membrane of the proximal tubule. *Am J Physiol Renal Physiol* 305: F734-F744, 2013.

20. **Kantarci S, Al-Gazali L, Hill RS, Donnai D, Black GC, Bieth E, Chassaing N, Lacombe D, Devriendt K, Teebi A, Loscertales M, Robson C, Liu T, MacLaughlin DT, Noonan KM, Russell MK, Walsh CA, Donahoe PK, and Pober BR**. Mutations in LRP2, which encodes the multiligand receptor megalin, cause Donnai-Barrow and facio-oculo-acoustico-renal syndromes. *Nat Genet* 39: 957-959, 2007.

21. **Kerjaschki D, and Farquhar MG**. Immunocytochemical localization of the Heymann nephritis antigen (GP330) in glomerular epithelial cells of normal Lewis rats. *J Exp Med* 157: 667-686, 1983.

22. **Kerjaschki D, and Farquhar MG**. The pathogenic antigen of Heymann nephritis is a membrane glycoprotein of the renal proximal tubule brush border. *Proc Natl Acad Sci USA* 79: 5557-5581, 1982.

23. **Ketteler M, Block GA, Evenepoel P, Fukagawa M, Herzog CA, McCann L, Moe SM, Shroff R, Tonelli MA, Toussaint ND, Vervloet MG, and Leonard MB**. Diagnosis, Evaluation, Prevention, and Treatment of Chronic Kidney Disease-Mineral and Bone Disorder: Synopsis of the Kidney Disease: Improving Global Outcomes 2017 Clinical Practice Guideline Update. *Annals of internal medicine* 168: 422-430, 2018.

24. **Kumar GC, M.; Faris, K.M.; Al Masri, O.** Renal involvement in a child with Donnai Barrow syndrome. *Asian J Pediatr Nephrol* 1: 93-95, 2018.
25. **Larsen T, Rontved CM, Ingvartsen KL, Vels L, and Bjerring M**. Enzyme activity and acute phase proteins in milk utilized as indicators of acute clinical E. coli LPS-induced mastitis. *Animal : an international journal of animal bioscience* 4: 1672-1679, 2010.
26. **Le Panse S, Galceran M, Pontillon F, Lelongt B, van de Putte M, Ronco PM, and Verroust PJ**. Immunofunctional properties of a yolk sac epithelial cell line expressing two proteins gp280 and gp330 of the intermicrovillar area of proximal tubule cells: inhibition of endocytosis by the specific antibodies. *EurJCell Biol* 67: 120-129, 1995.
27. **Leheste JR, Rolinski B, Vorum H, Hilpert J, Nykjaer A, Jacobsen C, Aucouturier P, Moskaug JO, Otto A, Christensen EI, and Willnow TE**. Megalin knockout mice as an animal model of low molecular weight proteinuria. *Am J Pathol* 155: 1361-1370, 1999.
28. **McCarthy RA, Barth JL, Chintalapudi MR, Knaak C, and Argraves WS**. Megalin functions as an endocytic sonic hedgehog receptor. *J Biol Chem* 277: 25660-25667, 2002.
29. **Morales CR, Zeng J, El AM, Barth JL, Chintalapudi MR, McCarthy RA, Incardona JP, and Argraves WS**. Epithelial trafficking of Sonic hedgehog by megalin. *J Histochem Cytochem* 54: 1115-1127, 2006.
30. **Nielsen R, Christensen EI, and Birn H**. Megalin and cubilin in proximal tubule protein reabsorption: from experimental models to human disease. *Kidney Int* 89: 58-67, 2016.
31. **Prabakaran T, Nielsen R, Larsen JV, Sorensen SS, Feldt-Rasmussen U, Saleem MA, Petersen CM, Verroust PJ, and Christensen EI**. Receptor-mediated endocytosis of alpha-galactosidase A in human podocytes in Fabry disease. *PLoS One* 6: e25065-e25076, 2011.
32. **Rieg T**. A High-throughput method for measurement of glomerular filtration rate in conscious mice. *JVisExp* e50330, 2013.
33. **Sahali D, Mulliez N, Chatelet F, Laurent-Winter C, Citadelle D, Sabourin JC, Roux C, Ronco P, and Verroust P**. Comparative immunochemistry and ontogeny of two closely related coated pit proteins. The 280-kd target of teratogenic antibodies and the 330-kd target of nephritogenic antibodies. *Am J Pathol* 142: 1654-1667, 1993.
34. **Schrauwen I, Sommen M, Claes C, Pinner J, Flaherty M, Collins F, and Van Camp G**. Broadening the phenotype of LRP2 mutations: a new mutation in LRP2 causes a predominantly ocular phenotype suggestive of Stickler syndrome. *Clinical genetics* 86: 282-286, 2014.
35. **Shaheen IS, Finlay E, Prescott K, Russell M, Longoni M, and Joss S**. Focal segmental glomerulosclerosis in a female patient with Donnai-Barrow syndrome. *Clin Dysmorphol* 19: 35-37, 2010.
36. **Shan J, Jokela T, Skovorodkin I, and Vainio S**. Mapping of the fate of cell lineages generated from cells that express the Wnt4 gene by time-lapse during kidney development. *Differentiation* 79: 57-64, 2010.
37. **Song J, Yu J, Prayogo GW, Cao W, Wu Y, Jia Z, and Zhang A**. Understanding kidney injury molecule 1: a novel immune factor in kidney pathophysiology. *American journal of translational research* 11: 1219-1229, 2019.
38. **Stora S, Conte M, Chouery E, Richa S, Jalkh N, Gillart AC, Joannis AL, and Megarbane A**. A 56-year-old female patient with facio-oculo-acoustico-renal syndrome (FOAR) syndrome. Report on the natural history and of a novel mutation. *Eur J Med Genet* 52: 341-343, 2009.
39. **Storm T, Christensen EI, Christensen JN, Kjaergaard T, Uldbjerg N, Larsen A, Honore B, and Madsen M**. Megalin Is Predominantly Observed in Vesicular Structures in First and Third Trimester Cytotrophoblasts of the Human Placenta. *The journal of histochemistry and cytochemistry : official journal of the Histochemistry Society* 64: 769-784, 2016.

40. **Storm T, Heegaard S, Christensen EI, and Nielsen R**. Megalin-deficiency causes high myopia, retinal pigment epithelium-macromelanosomes and abnormal development of the ciliary body in mice. *Cell Tissue Res* 99-107, 2014.
41. **Storm T, Tranebjaerg L, Frykholm C, Birn H, Verroust PJ, Neveus T, Sundelin B, Hertz JM, Holmstrom G, Ericson K, Christensen EI, and Nielsen R**. Renal phenotypic investigations of megalin-deficient patients: novel insights into tubular proteinuria and albumin filtration. *Nephrol Dial Transplant* 28: 585-591, 2013.
42. **Tauris J, Christensen EI, Nykjaer A, Jacobsen C, Petersen CM, and Ovesen T**. Cubilin and megalin co-localize in the neonatal inner ear. *Audiol Neurootol* 14: 267-278, 2009.
43. **Theilig F, Kriz W, Jerichow T, Schrade P, Hahnel B, Willnow T, Le HM, and Bachmann S**. Abrogation of Protein Uptake through Megalin-Deficient Proximal Tubules Does Not Safeguard against Tubulointerstitial Injury. *J Am Soc Nephrol* 18: 1824-1834, 2007.
44. **Vasli N, Ahmed I, Mittal K, Ohadi M, Mikhailov A, Rafiq MA, Bhatti A, Carter MT, Andrade DM, Ayub M, Vincent JB, and John P**. Identification of a homozygous missense mutation in LRP2 and a hemizygous missense mutation in TSPYL2 in a family with mild intellectual disability. *Psychiatric genetics* 26: 66-73, 2016.
45. **Vinge L, Lees GE, Nielsen R, Kashtan CE, Bahr A, and Christensen EI**. The effect of progressive glomerular disease on megalin-mediated endocytosis in the kidney. *Nephrol Dial Transplant* 25: 2458-2467, 2010.
46. **Weyer K, Storm T, Shan J, Vainio S, Kozyraki R, Verroust PJ, Christensen EI, and Nielsen R**. Mouse model of proximal tubule endocytic dysfunction. *Nephrol Dial Transplant* 26: 3446-3451, 2011.
47. **Willnow TE, Hilpert J, Armstrong SA, Rohlmann A, Hammer RE, Burns DK, and Herz J**. Defective forebrain development in mice lacking gp330/megalin. *Proc Natl Acad Sci USA* 93: 8460-8464, 1996.
48. **Yamazaki H, Saito A, Ooi H, Kobayashi N, Mundel P, and Gejyo F**. Differentiation-induced cultured podocytes express endocytically active megalin, a heymann nephritis antigen. *Nephron ExpNephrol* 96: e52-e58, 2004.
49. **Zheng G, Bachinsky DR, Stamenkovic I, Strickland DK, Brown D, Andres G, and McCluskey RT**. Organ distribution in rats of two members of the low-density lipoprotein receptor gene family, gp330 and LRP/alpa 2MR, and the receptor-associated protein (RAP). *J Histochem Cytochem* 42: 531-542, 1994.

690 **Figure legends**
691

692 **Figure 1.**

693 Renal function in megalin KO- and WT mice at 60 – 98 days. (A) GFR measured by FITC inulin
694 clearance. (B) Plasma creatinine. (C) Representative micrograph showing a megalin KO mouse
695 section stained with *Lotus* lectin illustrating normal proximal tubules sometimes interspaced by
696 areas lacking proximal tubules (arrow). Scale bars 50 µm. (D) Urinary NAGase excretion. (E)
697 Urinary KIM-1 excretion. The number of datapoints equals n.

698

699 **Figure 2.**

700 Localization of pathogenic variants in megalin and urinary profile of DB/FOAR patients and
701 carriers compared to controls. (A) Graphic depiction of megalin with domain organization and
702 identified pathogenic variants. (B) Urinary profile of the following proteins: RBP, albumin,
703 transferrin, β2-microglobulin, megalin, KIM-1, IgG and cystatin C. Values for each individual are
704 showed by the symbol from Table 1 and the horizontal line indicates the mean +/- SEM. The
705 number of datapoints equals n.

706

707 **Figure 3.**

708 Proximal tubule endocytic function and renal morphology in DB/FOAR patients and controls.
709 (A) Immunohistochemical staining for proximal tubule receptors and ligands in DB/FOAR
710 patients and controls. Scale bars 50 µm. (B) PAS staining and immunofluorescence analysis of
711 IgA of biopsy material from Patient 1-1 and 1-2. Patient 1-1 displays inflammation (arrowhead),
712 hypertrophic tubules (white arrow), tubular atrophy, and sclerotic glomeruli (black arrow).
713 Patient 1-2 displays a more well-preserved parenchyma. Scale bars: 200 µm.

714

715

716

717 **Fgure 4.**

Nephrogenesis in megalin KO- and WT mice at postnatal day four. (**A**) Micrograph of kidney sections from megalin KO and WT stained with *Lotus* lectin to identify the presence of the nephrogenic zone. Scale bars 200 µm. (B) Glomerular density at postnatal day four.

Figure 5.

Analyses of renal structure in megalin KO- and WT mice at 50-70 days. (A) Number of glomeruli. (B) Volume of glomeruli. (C) Distribution in percent of glomeruli volumes. (D) proximal tubule fraction in percent. (E) Total kidney volume. (F) Cortical volume. (G) Medullary volume. (H) Fraction of atubular glomeruli. In figure C, n=5 animals in each group encompassing 9-12,000 glomeruli. In all other figures n=the number of datapoints. Values for each individual mouse are showed by a symbol and the horizontal line indicates the mean +/- SEM.

Figure 6.

Schematic summary of the renal findings early in life of DB/FOAR patients and mice. In patients low GFR was detected, whereas urinary excretion of protein (UPC), albumin (UAC), high molecular weight proteins (Ig) and kidney injury marker, KIM-1 were elevated. In megalin KO mice we also found a lower GFR, elevated urinary excretion of kidney injury molecules (KIM-1 and NAG'ase), fewer glomeruli and increased number of atubular glomeruli (ATG).

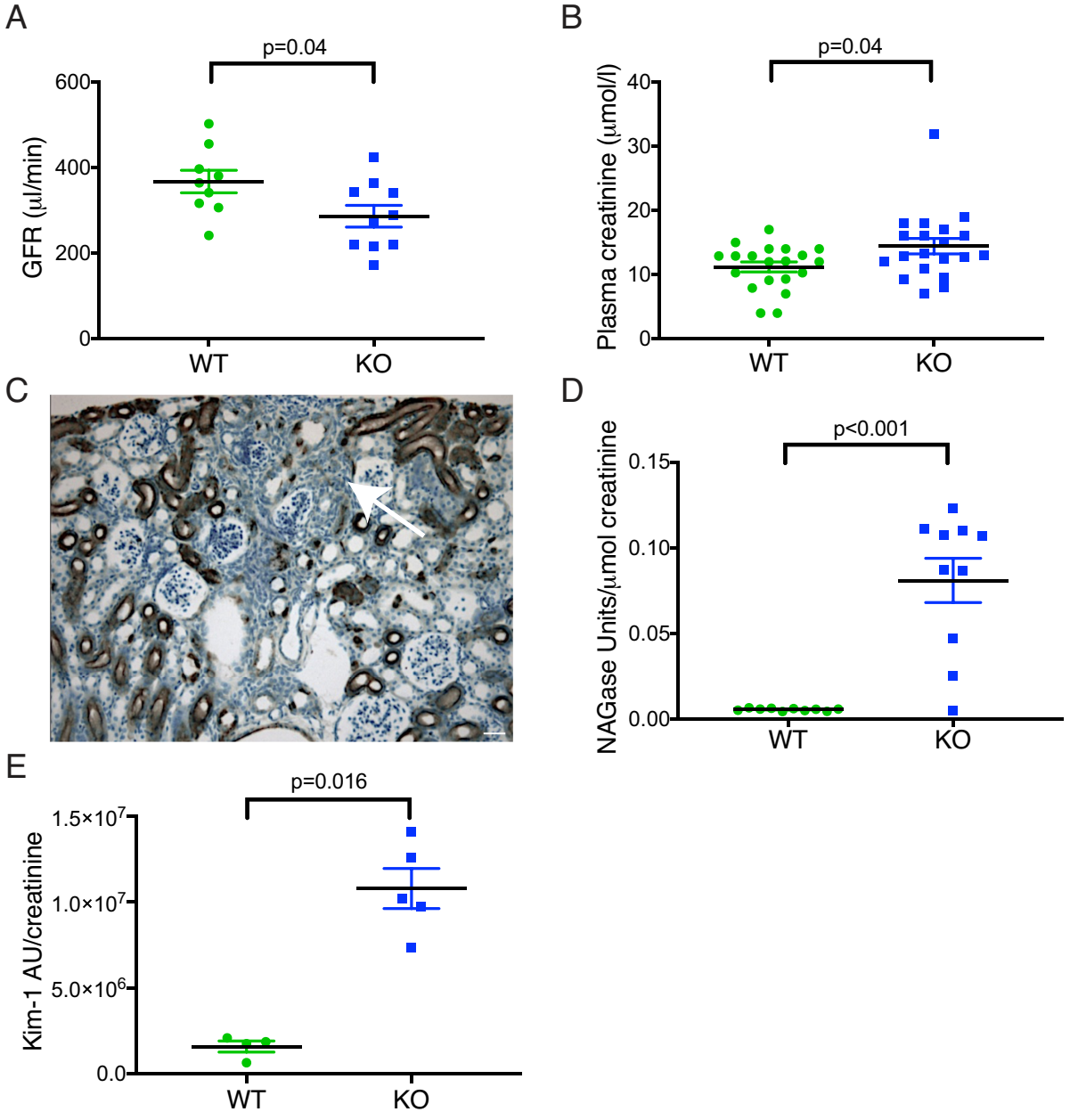
A
p=0.04
600
400
200
0
GFR (µl/min)
WT
KO
B
p=0.04
40
30
20
10
0
Plasma creatinine (µmol/l)
WT
KO
C
D
p<0.001
0.15
0.10
0.05
0.00
NAGase Units/µmol creatinine
WT
KO
E
p=0.016
1.5×10^7
1.0×10^7
5.0×10^6
0.0
Kim-1 AU/creatinine
WT
KO

Figure 1

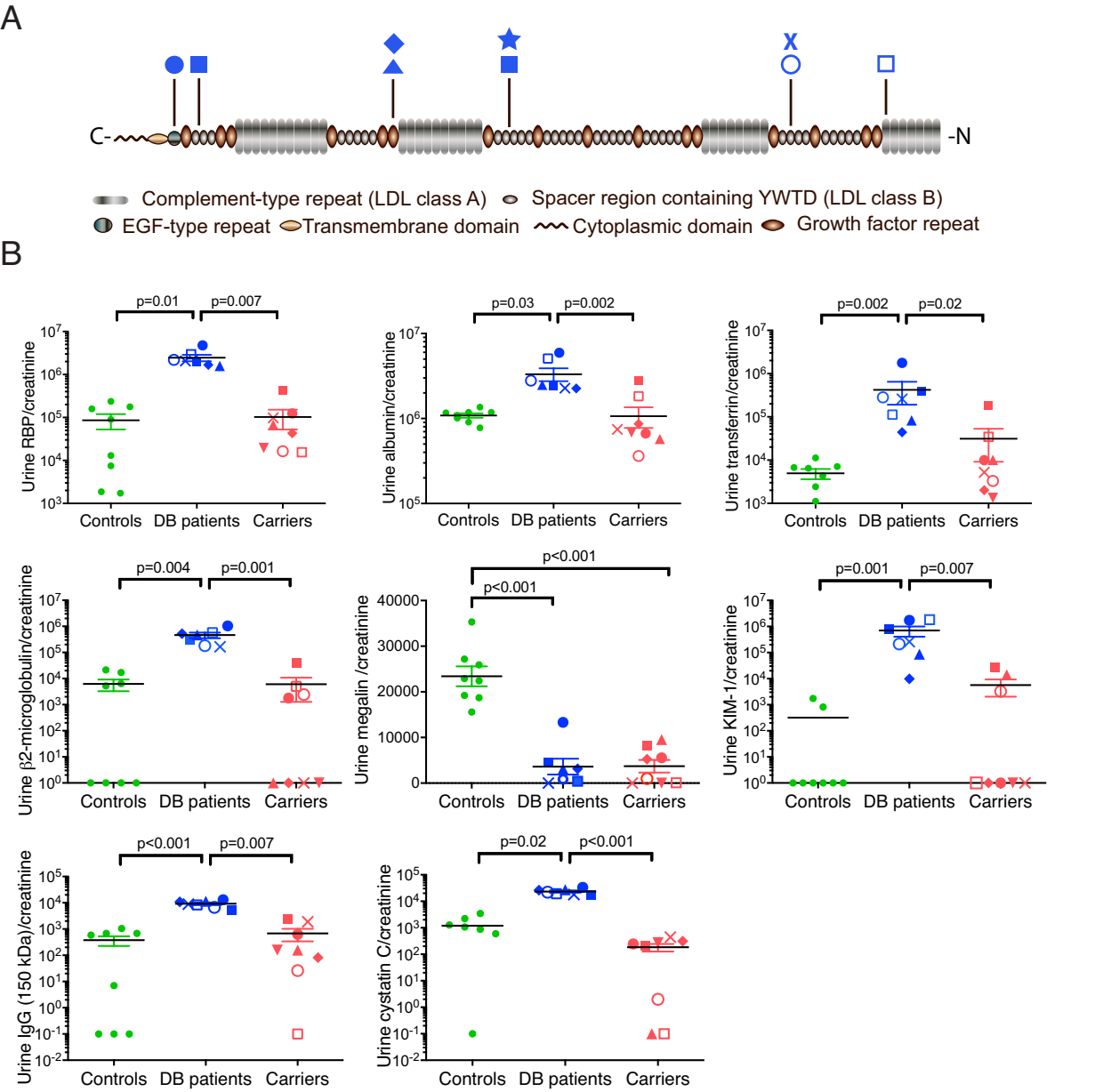
A
C-
-N
Complement-type repeat (LDL class A)
Spacer region containing YWTD (LDL class B)
EGF-type repeat
Transmembrane domain
Cytoplasmic domain
Growth factor repeat
B
Urine RBP/creatinine
p=0.01
p=0.007
Urine albumin/creatinine
p=0.03
p=0.002
Urine transferrin/creatinine
p=0.002
p=0.02
Urine β2-microglobulin/creatinine
p=0.004
p=0.001
Urine megalin /creatinine
p<0.001
p<0.001
Urine KIM-1/creatinine
p=0.001
p=0.007
Urine IgG (150 kDa)/creatinine
p<0.001
p=0.007
Urine cystatin C/creatinine
p=0.02
p<0.001
Controls
DB patients
Carriers

Figure 2

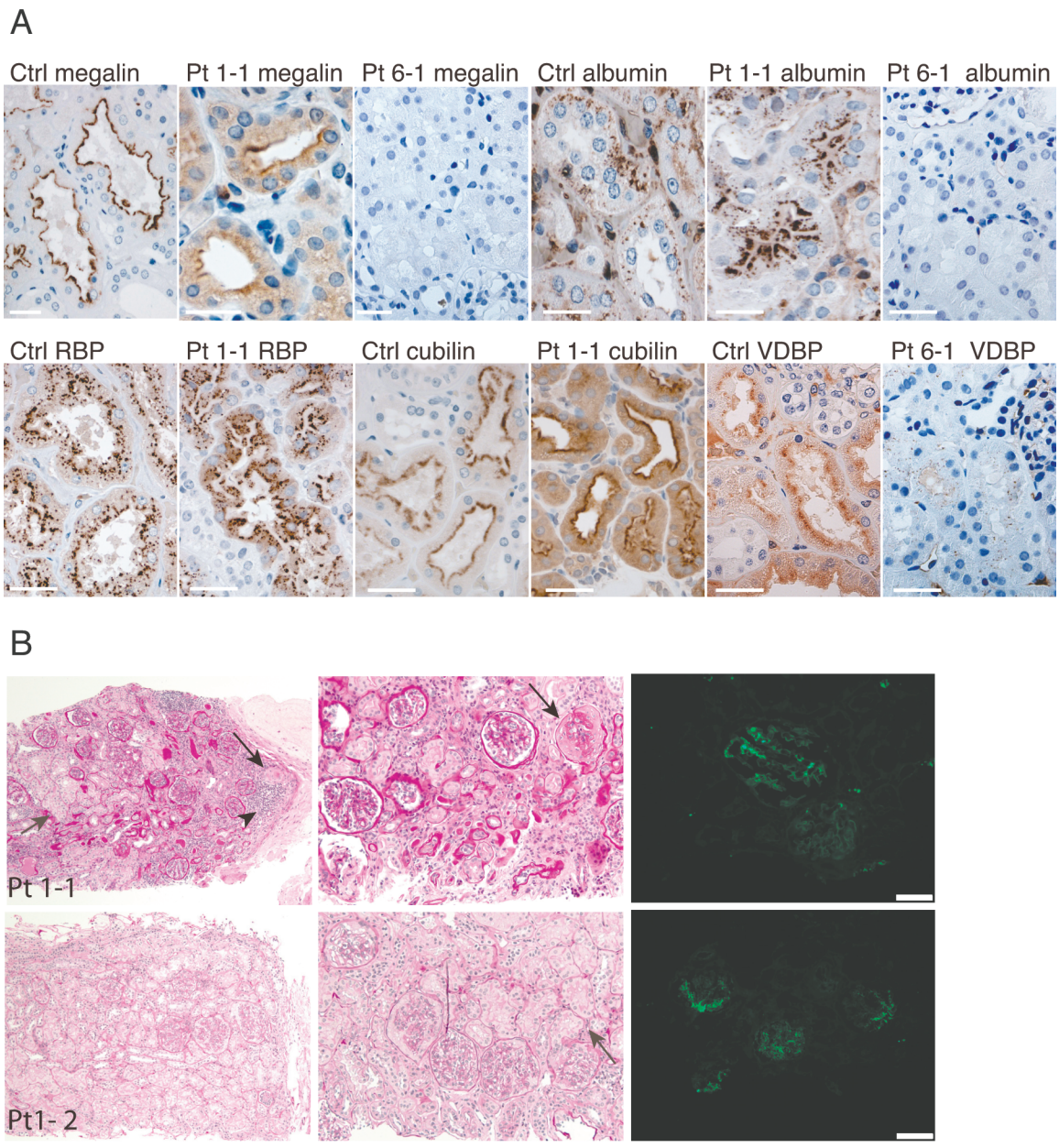
A
Ctrl megalin
Pt 1-1 megalin
Pt 6-1 megalin
Ctrl albumin
Pt 1-1 albumin
Pt 6-1 albumin
Ctrl RBP
Pt 1-1 RBP
Ctrl cubilin
Pt 1-1 cubilin
Ctrl VDBP
Pt 6-1 VDBP
B
Pt 1-1
Pt1- 2

Figure 3

A

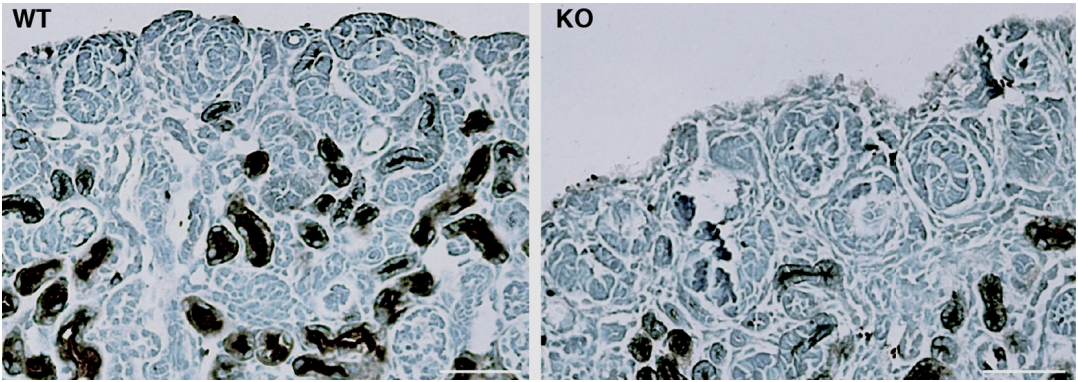

B

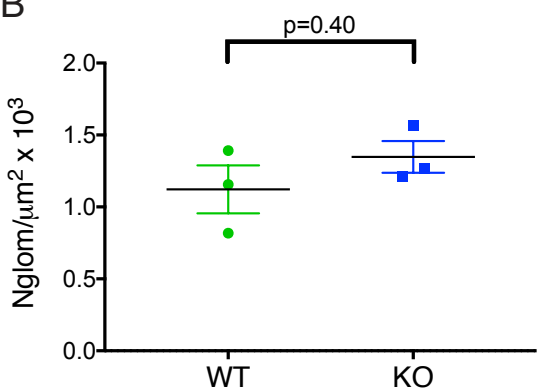

Figure 4

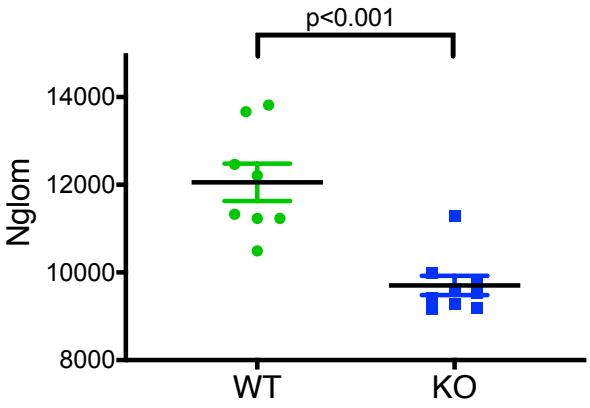
p<0.001
Nglom
14000
12000
10000
8000
WT
KO

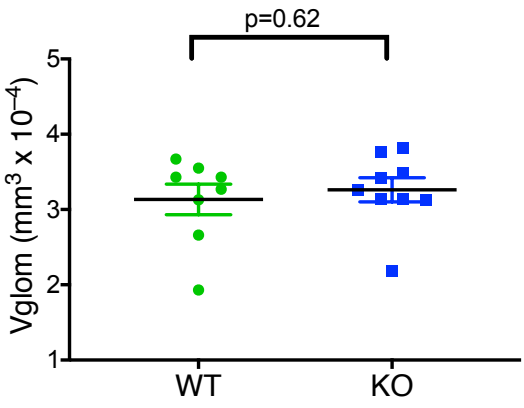
p=0.62
Vglom (mm3 x 10–4)
5
4
3
2
1
WT
KO

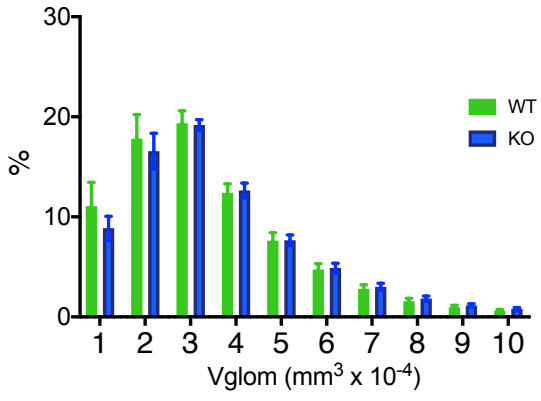
%
30
20
10
0
WT
KO
1 2 3 4 5 6 7 8 9 10
Vglom (mm3 x 10-4)

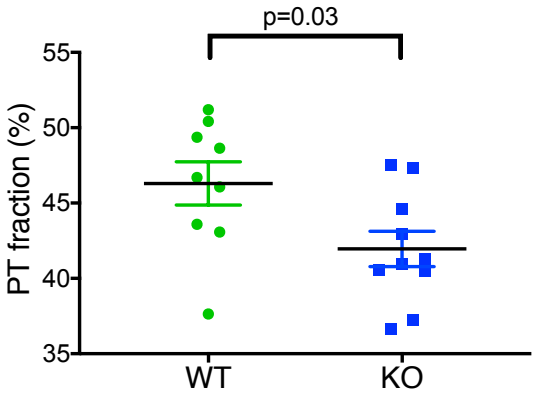
p=0.03
PT fraction (%)
55
50
45
40
35
WT
KO

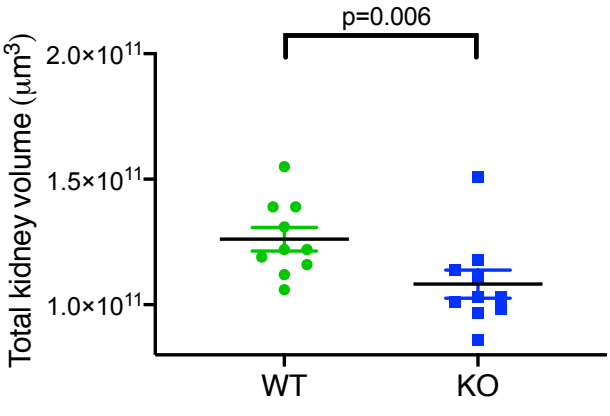
p=0.006
Total kidney volume (µm3)
2.0×10^11
1.5×10^11
1.0×10^11
WT
KO

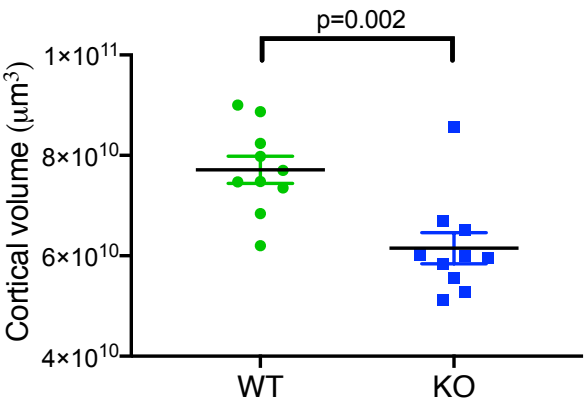
p=0.002
Cortical volume (µm3)
1×10^11
8×10^10
6×10^10
4×10^10
WT
KO

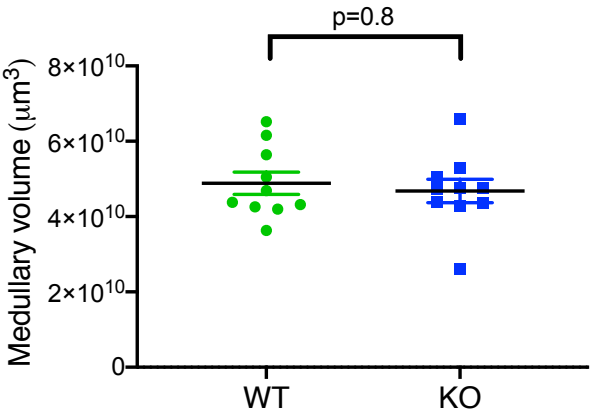
p=0.8
Medullary volume (µm3)
8×10^10
6×10^10
4×10^10
2×10^10
0
WT
KO

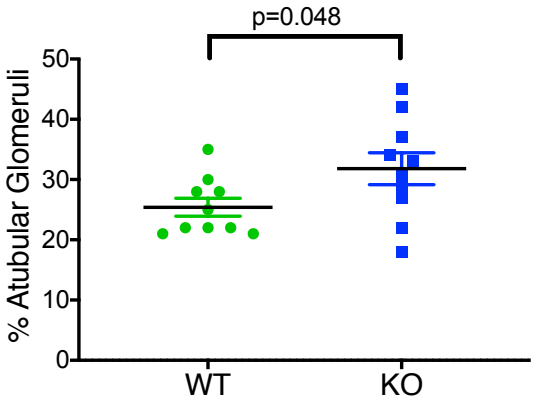
p=0.048
% Atubular Glomeruli
50
40
30
20
10
0
WT
KO

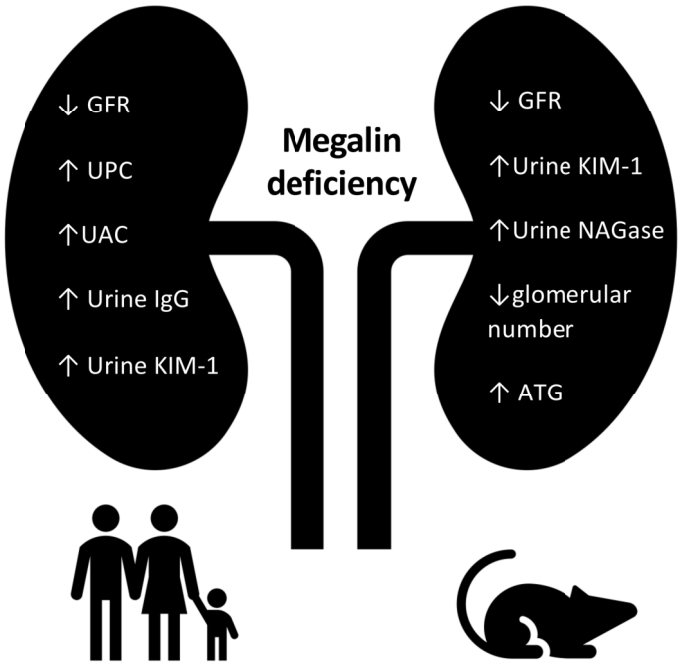
↓ GFR
↑ UPC
↑UAC
↑ Urine IgG
↑ Urine KIM-1
Megalin deficiency
↓ GFR
↑Urine KIM-1
↑Urine NAGase
↓glomerular number
↑ ATG

Figure 6

Beyond the tubule: Pathologic variants of *LRP2*, encoding the megalin receptor, result in glomerular loss and early progressive chronic kidney disease

DB patients

Mouse model of DB syndrome

Megalin dysfunction

- Urinary biomarkers
- Kidney function

Cationic ferritin

Perfusion fix

ex vivo CFE-MRI

OUTCOMES

DB patients

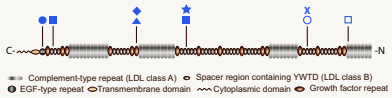

glomerulosclerosis

↑KIM-1

↑IgG

Mouse model of DB syndrome

↓GFR

↑NAGase

↓N_{glom}

CONCLUSION: Pathogenic variants in *LRP2* increase the risk of early onset of CKD. Disconnection of the glomerulo-tubular junction and nephron loss might be part of the underlying mechanism.

Patient	Symbol in figures	Gender	Age	Ethnicity	Pathogenic variant (homozygous)	UA/Crea. mg/mmol (ref: <3 mg/mmol)	UP/Crea. mg/mmol (ref: <15 mg/mmol)	Renal remarks
1-1	★	F	8 Y	UAE	c.7564T>C p.(Y2522H)	NA	260	Hematuria
1-2	★	F	4 Y	UAE	c.7564T>C p.(Y2522H)	NA	203	
2	□	M	35 Y	Portugal	c.857G>T p.(C286F)	10	166	CKD, azotemia, eGFR 17 ml/min/1.73m^2, 1.2-4.7 g protein/24h, occasionally hematuria, atrophic kidneys
3	■	F	12 Y	Belgium	c.7564T>C p.(Y2522H) & c.12623C>A p.(P4208H)	33	225	Normal renal morphology
4-1	✘	F	21 Y	Sweden	c.2639+1G>A (splicesite)	7	124	FSGS, eGFR <60 ml/min/1.73m^2
4-2	○	F	27 Y	Sweden	c.2639+1G>A (splicesite)	12	126	FSGS, eGFR <40 ml/min/1.73m^2
5	●	M	3 M	India	c.13139_13140insC	76	704	
6-1	▲	M	11 Y	Italy	c.9575G>A p.(R3192Q)	21	222	CKD, eGFR 68 ml/min/1.73m^2, mild phosphate leak, hypercalciuria
6-2	◆	F	14 Y	Italy	c.9575G>A p.(R3192Q)	16	221	eGFR 91 ml/min/1.73m^2, mild phosphate leak, hypercalciuria
Carrier	**Symbol in figures**	**Gender**	**Age**	**Ethnicity**	**Pathogenic variant (heterozygous)**	**UA/Crea. mg/mol**	**UP/Crea. mg/mmol**	**Renal remarks**
1a	★	M		UAE	c.7564T>C p.(Y2522H)	NA	28	
2a	■	M	62 Y	Portugal	c.857G>T p.(C286F)	9	46	Simple cyst left kidney
2b	□	F	56 Y	Portugal	c.857G>T p.(C286F)	9	15	Smaller pyelonephritic right kidney
2c	○	F	35 Y	Portugal	c.857G>T p.(C286F)	0.7	13	
2d	▲	F	33 Y	Portugal	c.857G>T p.(C286F)	5	19	
2e	●	F	21 Y	Portugal	c.857G>T p.(C286F)	4	17	
3a	✘	M	-	Belgium	NA	0.5	3	
4a	◆	M	-	Sweden	c.2639+1G>A (splicesite)	0.5	3	
4b	▼	F	-	Sweden	c.2639+1G>A (splicesite)	0.5	3	

Table 1. Biochemical - and genotype data of DB/FOAR patients and heterozygous carriers.